Asian Journal of Chemistry; Vol. 36, No. 3 (2024), 603-612

ASIAN JOURNAL OF CHEMISTRY

https://doi.org/10.14233/ajchem.2024.31059

Biogenic ZnO Nanoparticles Derived from *Garcinia gummi-gutta* Leaves: Synthesis, Characterization and its Multifaceted Applications

J.T. KURIAN and K.S. JOSEPH*

Department of Life Sciences, Christ University, Bangalore-560029, India

*Corresponding author: E-mail: joseph.ks@christuniversity.in

Received: 14 December 2023; *Accepted*: 19 January 2024; *Published online*: 28 February 2024; AJC-21550

The current study focused on the bioreduction synthesis of ZnO nanoparticles using *Garcinia gummi-gutta* leaf extracts. The UV-vis analysis of the nanoparticles has reported the formation of an SPR peak at 379 nm. The functional groups taking part in the reduction reaction were analyzed using the FTIR technique and the average crystalline size of ZnO nanoparticles were found to be 22.27 nm from XRD measurements. The SEM and TEM images revealed the hexagonal shape of the nanoparticles with an average size 72.78 nm and 71.91 nm, respectively. Further, the synthesized nanoparticles were reported to be efficient degradation reactive textile dyes. The photodegradation results reported 92-100% degradation of the reactive dyes within 80-320 min. The antibacterial efficacy of the nanoparticles was investigated and the MIC of the nanoparticles was found to be 100 µg/mL. The synthesized ZnO nanoparticles have exhibited significant cytotoxic effects on the MCF and HEP-G2 cell lines.

Keywords: Green synthesis, ZnO nanoparticles, Photocatalytic activity, Antimicrobial activity, Cytotoxic activity.

INTRODUCTION

The greener nanoparticle synthesis has gained popularity due to its cost-effectiveness, scalability, energy efficiency, simplicity and use of environmentally benign techniques [1]. Even though large-scale manufacturing of nanoparticles carried out by physical and chemical methods, the reduced toxic effects of the green nanoparticle acquire dominating concern for the research in different field applications [2]. The type of nanoparticle and the reducing and capping agents significantly affect the properties of the nanoparticle. The use of medicinal plants in the bio-fabrication of nanoparticles increases the medicinal value of the nanoparticles. Green synthesized nanoparticles are extensively studied for their photocatalytic, antimicrobial, anticancerous and antioxidant properties [3]. The tremendous changes happening in the global scenario generate hazardous threats to the health of both nature and humans. Industrialization has ultimately resulted in an increased number of highly contaminated water bodies, as effluents from industries such as textiles, paper, leather, food and pharmaceuticals are released into the environment without proper treatment [4]. Textile and dying industries are a major source of emerging organic pollutants that release effluents in the aqueous form without proper treatments. Reactive azo dyes, which are commonly used as colouring agents in the textile and dyeing industries, possess high molecular weight and are difficult to break down or remove from the aqueous phase [5,6]. The demand for novel effluent treatment methods is pressing, as the conventional effluent treatment methods are proving inadequate in fulfilling their intended purpose.

The employment of nanoparticles in the photocatalysis process has come under scrutiny recently due to benefits such as their superior macroscopic-scale properties, high surface-volume ratio and high surface energy. Recent studies on the biogenic nanoparticles have demonstrated that green synthesized metal oxide nanoparticles can effectively break down high molecular weight molecules and emerging pollutants without leaving harmful byproducts in the effluents [3,7-10]. Recently, Batra *et al*. [11] reported the review article on the efficient dye degradation strategies using green synthesized ZnO nanoparticles.

The evolution of multi-drug resistant microbes and the high exposure to carcinogenic compounds are two challenges of medical research. Due to their antibacterial activity, stable

robustness and long shelf life, certain inorganic metals and oxides, including zinc, copper, titanium, magnesium, and magnesium oxide, have been studied as possible antimicrobial agents [12]. Metals, exercising their antibacterial power, selectively disrupt the mechanism necessary for cell proliferation in Gram-positive and Gram-negative bacteria [13]. Due to its stability in hostile conditions, predominant antibacterial characteristics and low toxicity to humans, the ZnO nanoparticles are one of the most investigated inorganic metal oxide nanoparticles [14]. The bio-fabricated ZnO nanoparticle can be efficiently used as antimicrobial as well as anticancerous agents due to their nano-dimensions, high surface area, shape and the properties of the phytochemicals taken part in the green nanoparticles formulation [3,15].

The present study utilizes *Garcinia gummi-gutta* plant phytochemicals for the biofabrication of ZnO nanoparticles. *Garcinia gummi-gutta* commonly called Malabar tamarind is widely used for culinary purposes as well as medicinal purposes such as weight loss formulations. Hydroxy citric acid and garcinol, the main compounds present in the extract are studied for their antimicrobial and cytotoxic potentials [16]. Similar study explored the biosynthesis of ZnO nanoparticles using hydroxy citric acid, the primary component of *Garcinia* fruits derived from the dried rinds of *Garcinia gummi-gutta* [17]. In addition, comparison study on the green synthesis of silver nanoparticles utilizing the leaves of three different plants revealed that the fresh leaf extract from *Garcinia gummi-gutta* produced the best results [18]. Although *Garcinia gummi-gutta* seeds and fruits were used in the bioremediation and synthesis of ZnO and silver nanoparticles, but no research has been done on the plant's leaves for the production of ZnO nanoparticles and photocatalytic applications [16,19,20]. This study explored the potential applications of the *Garcinia gummi-gutta* leaf-mediated ZnO nanoparticles as potential photocatalytic, antimicrobial and anticancer agents.

EXPERIMENTAL

All the chemicals were obtained from Hi-media, Sigma Aldrich and Merck, USA. Reactive yellow-86, reactive blue-220, reactive blue-222 and reactive red-120 dyes were acquired from a textile industry, located at Jetpur city, India. Fresh leaves of *Garcinia gummi-gutta* (L) were obtained from the local fields of Kottayam, India. *Garcinia gummi-gutta* fresh leaves were shade-dried and ground using a grinder and reserved in air-tight containers at room temperature.

Plant extract preparation: The *Garcinia gummi-gutta* leaf powder (10 g) was added to 300 mL distilled water and refluxed at 50 ºC for 30 min. The resulting extract was filtered using Whatmann No. 1 filter paper and the filtered solution of *Garcinia gummi-gutta* leaf extract (GLE) was used for the biosynthesis of GLE-ZnO nanoparticles [7].

Biosynthesis of ZnO nanoparticles: In brief, 2 mL GLE was added to 50 mL zinc acetate dihydrate (0.5 M) and the pH of the reaction mixture was modified to 10-12 using NaOH. The colour of the reaction mixture was changed from light green to white precipitates demonstrating the evolution of ZnO nanoparticles. The reaction was continued in stirring conditions at room temperature for 1 h to complete the formation of biogenic ZnO nanoparticles. The solution was centrifuged at 10,000 rpm for 10 min, the supernatant was discarded and the pellets were collected and washed 5-6 times with water and ethanol to eliminate impurities. The washed pellets were resuspended in distilled water and dried in a hot air oven at 60 ºC [7]. The oven-dried nanoparticles were then calcinated at 500 ºC for 1 h [21].

Characterization: Biosynthesis of ZnO nanoparticles derived from *Garcinia gummi-gutta* leaves extract (GLE-ZnO NPs) were observed initially by UV- visible absorption spectroscopic technique (Shimadzu UV-1800ENG240V UV spectrophotometer) at a wavelength ranging from 200-800 nm. The biomolecules of GLE and the synthesized GLE-ZnO NPs were identified using a Shimadzu IR clubbed with reflectance QATR-S spectrophotometer at a scanning series of 4000-500 cm^{-1}. To analyze the crystal phase information of the biogenic GLE-ZnO NPs, XRD analysis was done using a Rigaku Miniflex X-ray using a Cu$K\alpha$ (λ = 1.54178 Å) radiation monochromatic filter in the range of 5-90º in 2θ with a scanning speed of 5º/min and the crystal size of the nanoparticles were evaluated using Debye-Scherrer's equation. The particle size and zeta potential analysis of the nanoparticles were done using Malvern zeta sizer ZEN3600 functioning by dynamic light scattering method. The surface morphology of the GLE-ZnO NPs was analyzed using ZEISS Sigma HV field emission scanning electron microscopy (FESEM) and EDX measurements were employed to examine the elemental composition of the GLE-ZnO nanoparticles. The size of the nanoparticles analyzed by SEM were calculated using Image J software (version: 1.53k). For a better understanding of the surface morphology and crystalline, the HRTEM-SAED analysis was also performed using JEOL JEM 2100 plus transmission electron microscope.

Antimicrobial analysis: The minimum inhibitory concentration (MIC) of the biogenic GLE-ZnO NPs against two different bacterial strains *viz. E. coli* (ATCC 10536) and *S. aureus* (ATCC 25923) and the fungal strains *C. tropicalis* (ATCC 10231) and *C. albicans* (ATCC 90028) was evaluated by broth dilution method by following the standard protocols of the Clinical Laboratory Standards Institute. The microbial strains were collected from the Microbial Type Culture Collection and Gene Bank (MTCC), Institute of Microbial Technology, IMTECH, Chandigarh, India. To produce the active cultures of the strains, the inoculated cells were subjected to overnight incubation at 37 ºC (120 rpm). The viability of cells was checked and the cultures were further cultured in Nutrient Broth (NB) and Potato Dextrose Broth (PDB) at 37 ºC for 24 h. The GLE-ZnO NPs were suspended in sterile distilled water and 10-300 µg/mL concentrations were prepared. In brief, 0.5 mL (1×10^5 cells mL^{-1}) microbial suspension was added to a 48-well Microtiter plate containing desired concentrations of GLE- ZnO NPs and the Nutrient Broth. The plate containing desired components was incubated at 37 ºC for 24 h. The absorbance was measured using a microtiter plate reader. The smallest fraction of the sample that suppressed the visible growth of the bacteria/fungi was treated as MIC/MCF values [22,23].

Cell cytotoxicity analysis: The cytotoxicity of biogenic GLE-ZnO NPs was evaluated on GEP-G2 and MCF cell lines. The procured stock cells were cultured in DMEM containing FBS, penicillin and streptomycin, at 37 ºC and 5% CO_2. The trypsinized cell culture cell count was adjusted to a cell count of 1.0×10^5 cells/mL by providing desired media containing 10% FBS. Diluted cell suspensions (100 µL, 50,000 cells/well) were added to a microtiter plate and incubated for 24 h till a partial monolayer was formed. The supernatant was scaled off and the monolayer was washed with the medium. A 100 µL of GLE-ZnO NPs were added to each well of the plate except the control wells and incubated at 37 ºC for 24 h in 5% CO_2. After the required incubation time supernatant from each well was separated and 100 µL DMSO was added. The formazan formed was solubilized and the absorbance was measured at 590 nm. The percentage of inhibition was measured and the IC_{50} value was evaluated using the dose-response curves of each cell lines [24,25].

$$\text{Growth inhibition (\%)} = \frac{\text{OD of the sample}}{\text{OD of the control}} \times 100$$

Photocatalytic degradation of textile dyes: Aqueous solutions of reactive textile dyes *viz*. reactive yellow-86 (RY-86), reactive blue-220 (RB-220), reactive blue-222 (RB-222) and reactive red-120 (R-120) were employed to investigate the photocatalytic degradataion efficiency of the GLE-ZnO NPs. In brief, 10 mg of GLE-ZnO NPs (1 mg/mL) was added to 10 mL of corresponding dye solutions (5 ppm) and the dye formulations without the addition of nanoparticles was taken as control. The GLE-ZnO NPs and the dye solutions were mixed using a magnetic stirrer in dark for 10-15 min and subjected to the UV irradiation for 320 min with constant stirring. The absorbance of each dye was analyzed using a UV-Vis spectrophotometer at regular time intervals *viz.* 0, 5, 10, 20, 40, 80, 160 and 320 min to monitor the progress of the reaction. The rate of degradation of reactive dyes by biogenic GLE-ZnO NPs was calculated using the following formula [7]:

$$\text{Degradation (\%)} = \frac{C_o - C_t}{C_o} \times 100$$

where C_o and C_t are the absorbances of the control and test respectively.

Bioefficiency analysis of treatment: The toxicity reduction and the degradation efficiency of the GLE-ZnO NPs-treated dyes were monitored at different trophic levels. *Vigna radiata* growth inhibition test was performed as previously performed [26] with few modifications. *Vigna radiata* seeds were sprouted in distilled water and 10 sprouts were taken and introduced into 10 mL treated, untreated dyes and GLE-ZnO NPs (1 mg/mL) solutions. Seedling exposed to distilled water was taken as control. After 4-5 days of exposure, the percentage of leaf, stem and root growth inhibition was calculated.

$$\text{Growth inhibition (\%)} = \frac{L_o - L_t}{L_o} \times 100$$

where L_o = length (leaf/stem/root) of control, L_t = length (leaf/stem/root) of test.

The brine shrimp lethality study was carried out using the reported methods [27,28] with slight modifications. *Artemia salina* (L.) eggs were hatched in artificial seawater (36 g rock salt in 1 L deionized water). 20 Nauplii along with 5 mL artificial sea water was exposed to 5 mL of treated and untreated dye solutions as well as GLE-ZnO NPs solution in test tubes. Artificial seawater with 20 nauplii was kept as control. The setup was left uncovered under constant light source at room temperature. After 24 h of exposure, the number of surviving shrimps was counted and the lethality percentage was calculated.

$$\text{Mortality (\%)} = \frac{\text{Number of dead nauplii}}{\text{Total number}} \times 100$$

RESULTS AND DISCUSSION

Plant phytochemicals are frequently utilized as reducing agents in the synthesis of non-toxic nanoparticles. The plant phytochemicals used in the synthesis process significantly influence the physical attributes of the nanoparticles, such as their size, shape and crystallinity [7,29]. The current study investigates the potentiality of the leaf extracts of *Garcinia gummi-gutta* in the bioreduction of ZnO nanoparticles. The synthesized nanoparticles were characterized by different spectroscopic and microscopic techniques.

UV-visible studies: Fig. 1 depicts the UV-vis spectrum of the synthesized GLE-ZnO NPs. A characteristic SPR peak was observed at 379 nm in the UV-vis spectra of the biosynthesized nanoparticles, suggesting the existence of ZnO nanoparticles [20]. According to Jain *et al*. [29], a successful process can be determined by the highest absorbance of ZnO NPs produced by *Serratia nematodiphila* ZTB15 at 379 nm, which is consistent with the data obtained. Moreover, the formation of SPR peaks can be considerably influenced by the type of precursor and the calcination temperature [30]. The band gap energy of the GLE-ZnO NPs was measured using Wood-Tauc's relation and found to be 2.79 eV, indicating that the synthesized GLE-ZnO NPs have an efficient potential in the photodegradation of textile dye molecules [31].

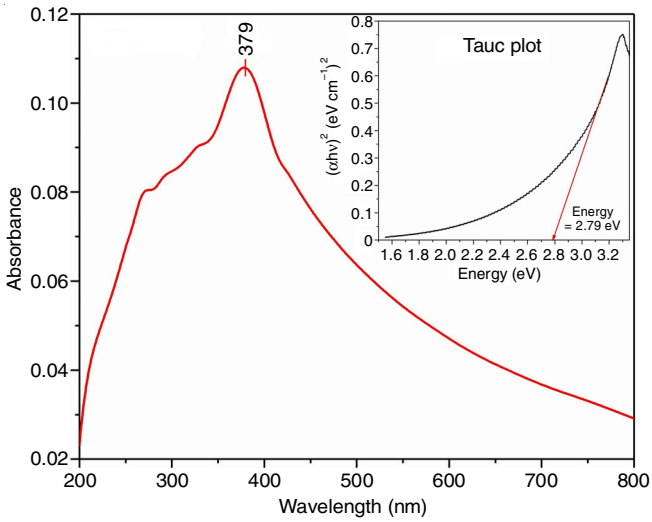

Fig. 1. UV-vis spectrum-Tauc's plot of the synthesized GLE-ZnO NPs showing the SPR peak of the GLE-ZnO NPs at 379 nm and the bandgap energy of the GLE-ZnO NPs

FTIR studies: FTIR spectrum of the leaves extract and the synthesized GLE- ZnO NPs were analyzed to evaluate the biomolecules taken apart in the green synthesis of GLE-ZnO NPs (Fig. 2). The FTIR spectra of GLE demonstrated the presence of the characteristic peaks at 3726.17 and 2903.94 cm^{-1} indicating the presence of O-H stretching of alcohol and C-H stretching of alkenes, respectively. The peaks at 2838.62 and 1718.23 cm^{-1} represent the presence of C-H stretching of aldehyde and C=O stretching of carboxylic acid. Similarly, intrinsic peaks were observed at 1591.44, 1434.68, 1360.91, 12.74.84, 1035.86 and 876.02 attributing the presence of N-O stretching of nitro compounds, O-H bending of carboxylic acids, S=O stret-ching and C-O stretching of aryl ether, S=O stretching of sulfoxide and the C-H bending, respectively. These peaks validated the presence of flavonoids, anthocyanins and phenols in the leaves extract of*Garcinia gummi-gutta* [32]. Similarly, the FTIR spectrum of the GLE-ZnO NPs revealed the presence of intrinsic peaks at 3743.37, 2965.94, 1679.33, 1516.76 cm^{-1} attributing the existence of O-H stretching of alcohol, C-H stretching of alkane, C=O stretching of conjugated ketone and the N-O stretching of nitro compounds, respectively in the synthesized GLE-ZnO NPs. Moreover, the peaks at 879.84 and 616.25 cm^{-1} are due to the C=C bending of alkene and the metal oxide bond [20], whereas the peak at 1679.33 cm^{-1} may be due to the presence of hydroxy citric acid, the major component present in the *Garcinia* extract that helps in the reduction of Zn ions [33]. Thus, a significant change in the intensity of the peaks was observed in the GLE-ZnO nanoparticle spectrum due to the participation of the biomolecules in the green synthesis process [34].

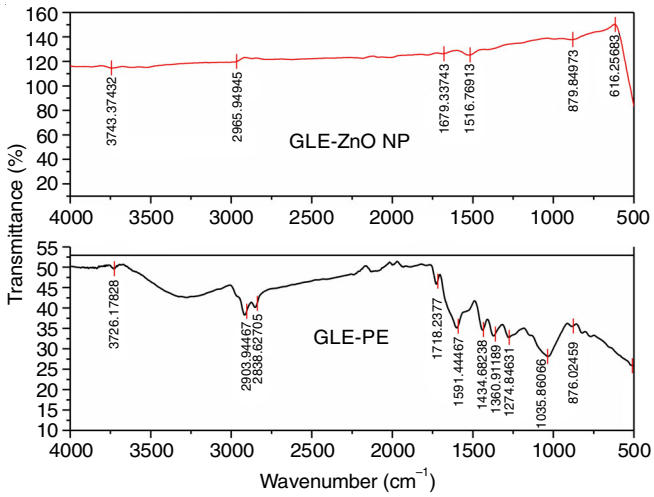

Fig. 2. FTIR spectra of the *Garcinia gummi-gutta* leaf extract and the synthesized GLE-ZnO NPs

XRD studies: The intense peaks of the GLE-ZnO NPs confirmed the crystallinity of the synthesized nanoparticles. The XRD spectrum of the biosynthesized nanoparticles displayed diffraction peaks at 31.74º, 34.41º, 36.22º, 47.58º, 56.57º, 62.83º, 67.88º, 69.10º, 72.54º and 77.02º attributing the hexagonal planes of (100), (002), (101), (102), (110), (103), (112), (201), (004) and (002), respectively [20] (Fig. 3). The observed planes of the GLE-ZnO NPs represent the hexagonal

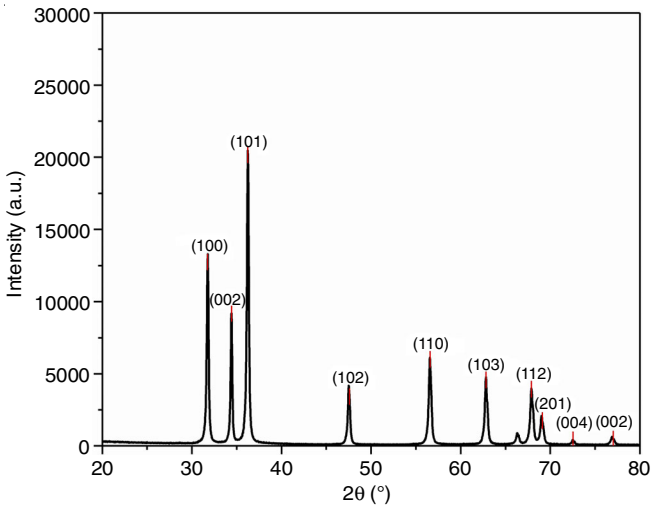

Fig. 3. XRD analysis revealing the planar values of the hexagonal wurtzite-shaped GLE-ZnO NPs

wurtzite phase of ZnO nanoparticles (JCPDS card no. 36-1451). The GLE-ZnO NPs had an average crystallite size of 22.27 nm, as determined by using Debye Scherrer's equation [32].

Dynamic light scattering (DLS) analysis: DLS analysis of the synthesized nanoparticles was done to analyze the fluctuations in the light intensity by the GLE-ZnO NPs [35]. The particle size of the GLE-ZnO NPs was observed as 78.17 nm. Also, the presence of a larger peak was found at 444.1 nm due to the aggregation of the green nanoparticles. Because of the formation of the agglomerated nanoparticles, the average diameter of the particle was found to be 313.0 nm with a PDI value of 0.413. Fig. 4 represents the DLS study of the synthesized GLE- ZnO NPs. Zeta potential analysis of the nanoparticles was done to understand the charge dispersal and the stability of the nanoparticles was found to be –21.5 mV substantiating the stability of the synthesized ZnO nanoparticles in the colloidal solution. The particles with large negative or positive zeta potential values exhibit less agglomeration of the particles as the particles tend to repel each other. Due to the low negative charge of the GLE-ZnO NPs, which is less than -30, the particles have a greater tendency to aggregate. The reason is attributed due to the reduced repulsive force that would normally inhibit their agglomeration [36].

Morphological studies: The exterior morphology of the GLE-ZnO NPs was analyzed using FESEM analysis. Fig. 5 represents the FESEM-EDX images of the GLE-ZnO NPs at different magnifications. The FESEM image of biogenic ZnO nanoparticles discovered the hexagonal shape with varying sizes from 58-92 nm. The average particle size of the ZnO nanoparticles was found to be 72.78 nm using ImageJ software. The varying sizes of the nanoparticles may be due to the polarity and the electrostatic attraction of the particles as depicted in the DLS analysis. The elemental configuration of the biogenic ZnO NPs was analyzed by EDX technique. The EDX spectrum displayed peaks for zinc, oxygen and carbon with atomic percentages of 31.53%, 38.42% and 30.06%, respectively substantiating the establishment of ZnO nanoparticles. The presence of carbon element may be due to the phytochemicals used in the bioreduction of GLE-ZnO NPs.

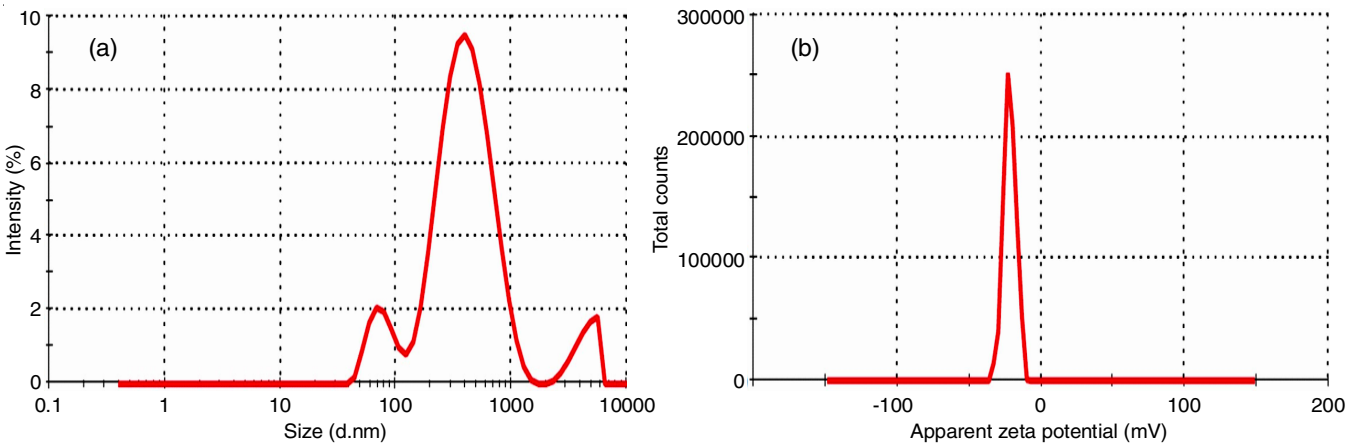

Fig. 4. DLS analysis of the GLE-ZnO NPs; (a) particle size, (b) zeta potential analysis of the synthesized GLE-ZnO NPs

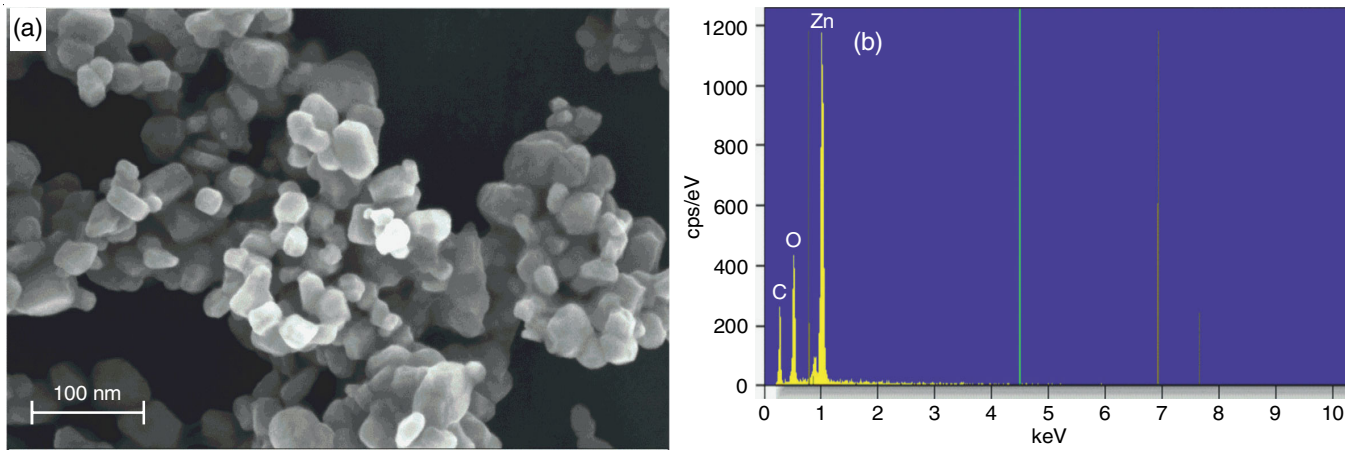

Fig. 5. SEM-EDX analysis of the GLE-ZnO NPs; (a) SEM images of the GLE-ZnO NPs displaying the hexagonal shaped NPs, (b) EDX analysis of the GLE-ZnO NPs displaying the peaks of Zn, O and C

TEM studies: Fig. 6 represents the TEM-SAED images of the GLE-ZnO NPs, which indicate the hexagonal-shaped nanoparticles with an average size of 71.91 nm similar to the size attained from SEM analysis. Moreover, the investigation of SAED patterns confirmed the crystallinity of the GLE-ZnO NPs observed as in XRD analysis. Inspection of *d*-spacing values obtained from TEM-SAED patterns-concentric rings validated the hexagonal wurtzite phase of the GLE-ZnO NPs [32].

Antimicrobial activity: Antimicrobial activity and the determination of MIC of the GLE-ZnO NPs were carried out using two bacterial strains *viz*. *S. aureus* (ATCC 25923) and

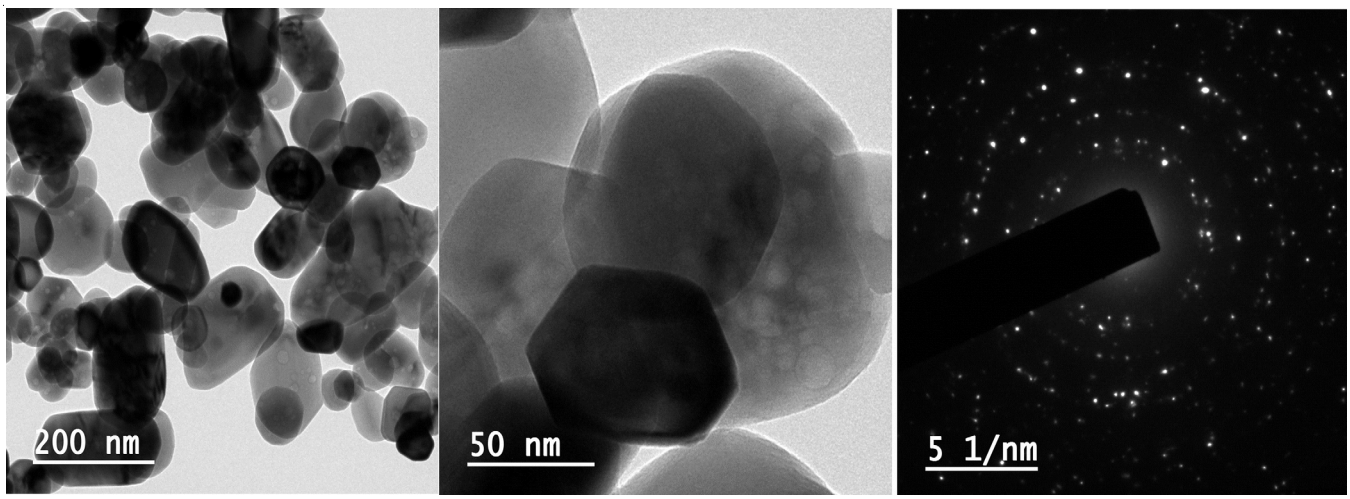

Fig. 6. TEM-SAED images of the GLE-ZnO NPs

TABLE-1
MINIMUM INHIBITORY CONCENTRATION OF GLE-ZnO NP AGAINST DIFFERENT MICROBIAL STRAINS

Microorganism	Microbial strains	IC_{90} (µg/mL)	MIC (µg/mL)	MIC inhibition (%)
Bacteria	*S. aureus* (ATCC 25923)	48.12	100	97.32
	E. coli (ATCC 10536)	30.24	100	96.27
Fungi	*Candida albicans* (ATCC 90028)	30.13	100	94.33
	Candida tropicalis (ATCC 10231)	48.84	100	95.34

E. coli (ATCC 10536) and two fungal strains *viz*. *C. albicans* (ATCC 90028) and *C. tropicalis* (ATCC 10231). Fig. 7 represents the percentage of microbial growth inhibition exhibited by the different concentrations (20-100 µg/mL) of GLE-ZnO NPs. It shows the efficient antimicrobial efficiency of the GLE-ZnO NPs. *E. coli* exhibited higher susceptibility (IC_{90} - 30.24 µg/mL) against GLE-ZnO NPs than *S. aureus* observed an IC_{90} value of 48.12 µg/mL. The superior susceptibility of Gram-negative strains by the nanoparticles may be due to the difference in the cell wall configuration of Gram-negative and Gram-positive species [37]. The synthesized nanoparticles have displayed antifungal activity against *C. albicans* and *C. tropicalis* with IC_{90} values of 30.13 µg/mL and 48.84 µg/mL, respectively (Table-1). The antimicrobial action of the metal oxide nanoparticles involves the release of metal ions, which are absorbed by microbial cell membranes and cause interactions with functional groups of protein and nucleic acid, limiting enzyme activity. As a result, the cell structure changes, ultimately inhibiting the microbe. Along with these, metal oxide nanoparticles also exert their effects through the generation of reactive oxygen species (ROS), which leads to electrostatic contact and changes in the prokaryotic cell wall, enzymes or DNA pathways [13].

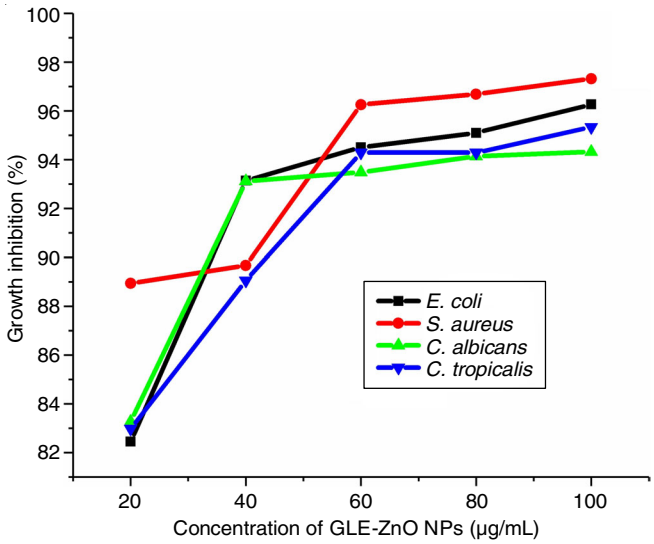

Fig. 7. Graphical depiction of the antimicrobial activity of GLE-ZnO NPs demonstrating the percentage growth inhibition of the bacterial and fungal stains at different concentrations of the GLE-ZnO NPs

Cell cytotoxicity studies: The anticancerous activity of the GLE-ZnO NPs was studied employing MTT assay on Liver cancer cell lines (Hep-G2) and Mammalian breast cancer cell lines (MCF cell lines). The *in vitro* cell cytotoxic activity of varying concentrations of GLE-ZnO NPs (10-100 µg) was observed and a sigmoid dose-dependent curve was formulated to find the IC_{50} values. The IC_{50} values of biogenic GLE-ZnO NPs were calculated as 51.75 ± 0.05 µg/mL on Hep-G2 and 49.75 ± 0.05 µg/mL on MCF cell lines (Table-2). The cell lines treated with nanoparticles have displayed cell disruptions representing the cytotoxic potentials of the nanoparticles, whereas the control cell lines maintained their intact structure and shape (Fig. 8). The cell cytotoxicity of the GLE-ZnO NPs may be ascribed to the biomolecules present in the *Garcinia gummi-gutta* leaf extract. The major phytochemicals present in the leaves extract *viz*. hydroxy citric acid and garcinol have proven to have cytotoxic potential against liver cancer cells and breast cancer cells [38]. In addition to that, the desired surface-to-volume ratio of these nanosized particles increases the possibilities of penetration as well as the cytotoxic response of the nanoparticles. The studies on the mechanism of the anticancerous activities of the nanoparticles have proven the possibilities of paraptosis, DNA damage, radio sensitizing, autophagy, oxidative stress stimulation, initiation of carcinogen detoxifying-activation enzymes or arresting the cancer cell cycle [39].

TABLE-2
INHIBITION OF CELL VIABILITY OF CELL LINES BY GLE-ZnO NPs

Concentration of NPs (µg)	Cell viability (%)	
	Hep-G2	MCF-7
0	100	100
10	92	95
20	84	86
30	75	78
40	63	62
50	54	49
60	42	42
70	33	36
80	23	23
90	18	19
100	10	10

Photocatalytic degradation studies: The photocatalytic activity of the GLE-ZnO NPs under UV-irradiation has been investigated by the UV-visible spectrum studies. Initially, the maximum absorption wavelength of the reactive dyes was found to be 421, 667, 598 and 508 nm, respectively for RY-86, RB-220, RB-222 and R-120. Reduction in the absorption intensity of the dye solution was investigated to determine the degradation of the studied dyes. The photodegradation of RY-86, RB-220, RB-222 and R-120 as a function of time is illustrated in Fig. 9. Reactive yellow-86 (RY-86) dye has shown 100% degradation between 80-160 min of UV-irradiation, while reactive blue-220 (RB-220) dye has shown 99.48% degradation within 80 min of exposure. Following that reactive blue-222 (RB-

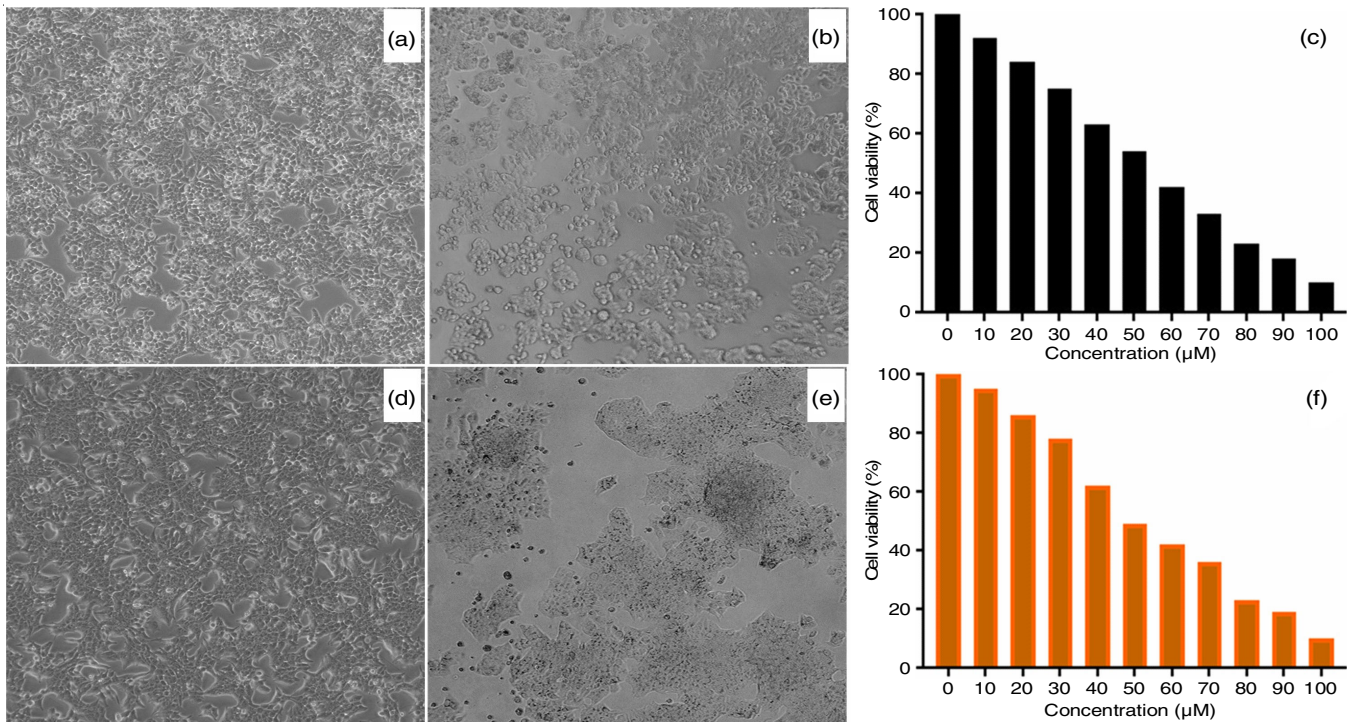

Fig. 8. *In vitro* cell cytotoxicity studies of GLE-ZnO NP against Hep G2, MCF cell lines. (a) Hep-G2 control cell lines, (b) GLE-ZnO NP treated Hep-G2, (c) graphical representation of cell viability inhibition of Hep-G2 cell lines on treatment with GLE-ZnO NPs (20-100 µg), (d) MCF control cell lines, (e) GLE-ZnO NP treated MCF cell lines, (f) graphical representation of cell viability inhibition of MCF cell lines on treatment with GLE-ZnO NPs (20-100 µg)

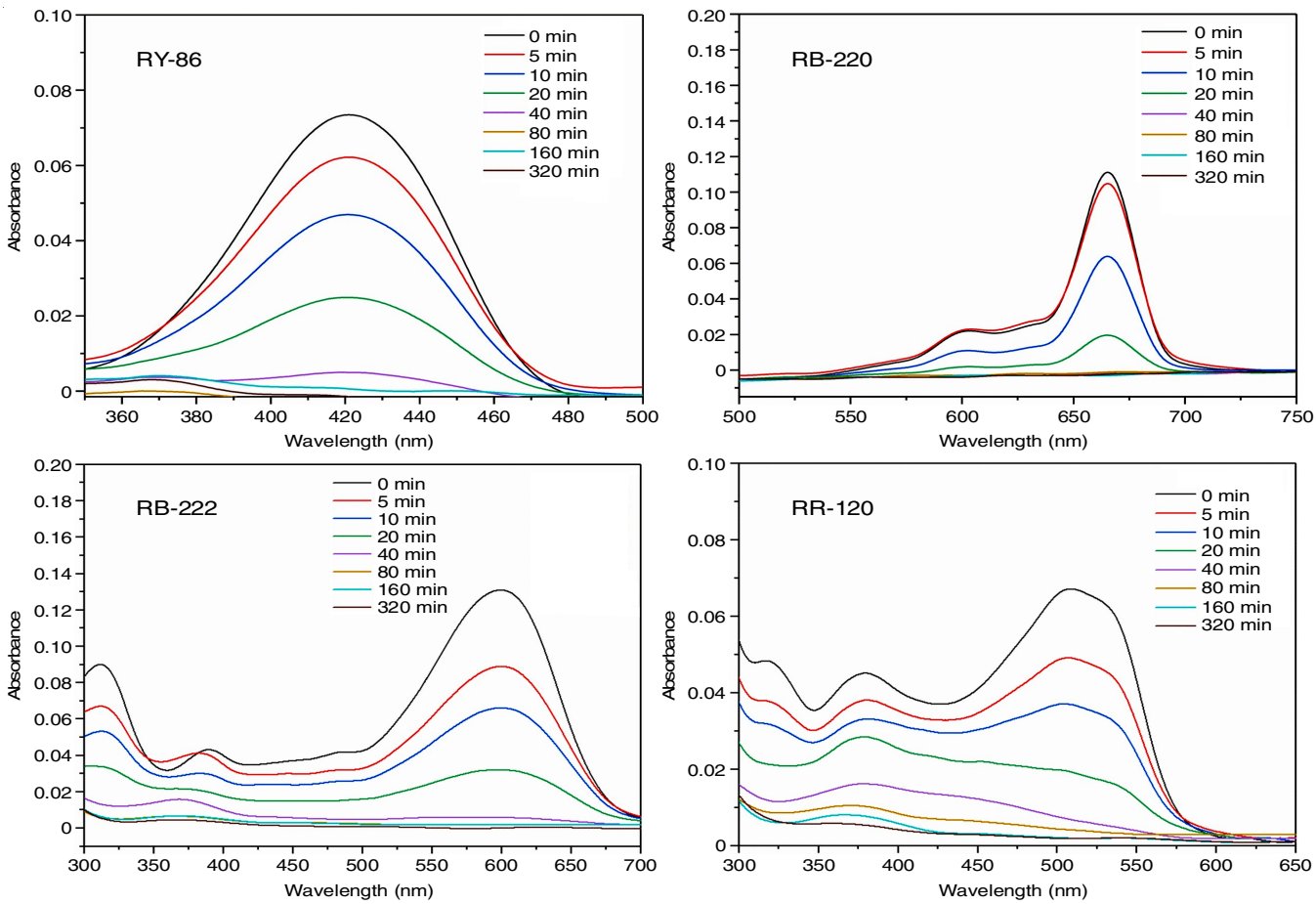

Fig. 9. UV absorption spectrum demonstrating the photocatalytic degradation of textile dyes by the GLE-ZnO NPs

222) and reactive red-120 (RR-120) have shown 96.95% and 92.5 % degradation efficiency at 320 min (Table-3).

TABLE-3
PHOTOCATALYTIC DEGRADATION POTENTIAL OF GLE-ZnO NPs ON REACTIVE TEXTILE DYES

Dye	Maximum absorbance (nm)	Degradation (%)	Time (min)
RY-86	421	100	80-160
RB-220	667	99.48	80
RB-222	598	96.95	320
R-120	508	92.5	320

Bioefficiency analysis of treatment

***Vigna radiata* growth inhibition test:** As the dye effluents from the textile industries are released into water bodies, the toxic dye pollutants can significantly affect the flora and fauna of the aquatic ecosystem. The efficiency of the photocatalytic treatment of the dye solutions with the nanoparticles was analyzed by evaluating the effect of the untreated dye molecules on the growth of aquatic plants and the evaluation of the reduction in the toxicity of the nanoparticle-treated solutions. The effect of untreated and treated dye solutions as well as the synthesized nanoparticles on the growth of green gram sprouts was analyzed in terms of growth inhibition of leaf, shoot, root and total length. As observed in Table-4, the untreated dye solutions exhibited high toxicity in terms of a high rate of growth inhibition of the leaf, stem and root as well as the total length of the green gram sprouts. Meanwhile, the nanoparticle-treated solutions have shown a significant reduction in toxicity as the inhibition of the growth of the leaf, stem, root and total length was significantly reduced as compared to the untreated dye solutions (Fig. 10). Similarly, the effect of synthesized nanoparticles on the growth of green gram growth was also analyzed, the obtained results have shown negligible toxicity of the green synthesized GLE-ZnO NPs on the plant growth indices.

Brine shrimp lethality assay: The toxic effects of the textile dye molecules on the aquatic fauna were examined by using the brine shrimp lethality assay. The mortality rate of brine shrimp nauplii exposed to untreated and treated dye solutions was done to analyze the toxic effects of the reactive dyes on brine shrimp as well the effectiveness of the nanoparticle treatment in diminishing the detrimental effects of the dye effluents on the aquatic organisms. Table-4 shows the increased mortality

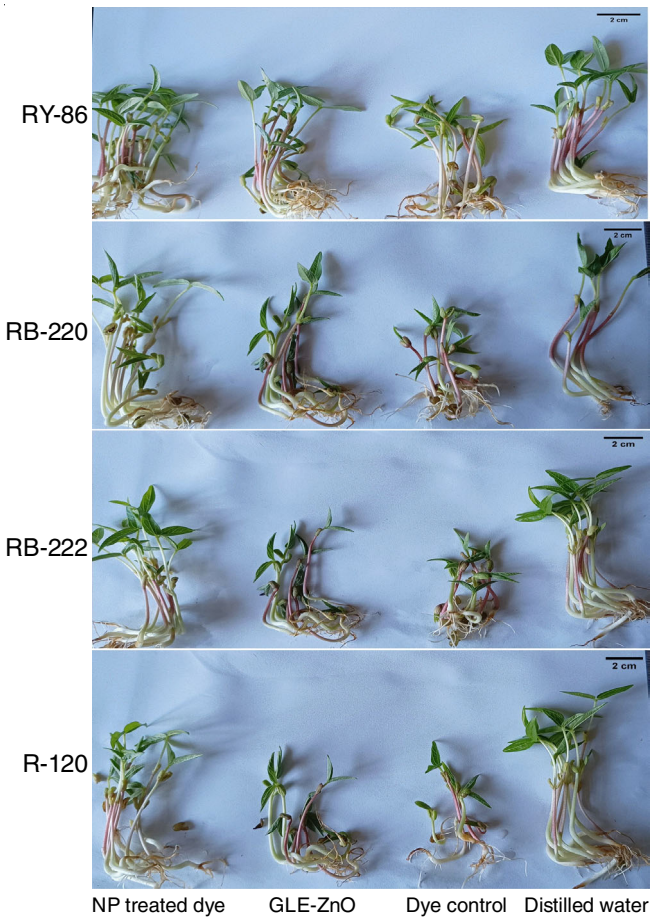

Fig. 10. Images demonstrating the effect of the untreated, treated dyes and the synthesized GLE-ZnO NPs on *Vigna radiata* sprouts growth

rate of brine shrimp nauplii by the reactive dye solutions as well as the reduction in the mortality rate by the treatment of the respective dye solutions with GLE-ZnO NPs. The brine shrimp exposed to the untreated dye solutions reported a high mortality rate. That was reduced significantly after treating the dye solutions with the green synthesized GLE-ZnO NPs revealing the efficient degradation of the dye compounds. The microscopic examination of the brine shrimp nauplii after exposure to the untreated dye solutions has shown the uptake of dye molecules to the digestive canal of the nauplii as well as the cell disruptions caused by the dye molecules (Fig. 11). The nauplii exposed to the photodegraded solutions reported

TABLE-4
TOXICITY ANALYSIS OF GLE-ZnO NP TREATED DYES

Conditions	*Vigna radiata* growth inhibition (%)				Brine shrimp lethality
	Leaf	Stem	Root	Total	Mortality (%)
Distilled water	0.00 ± 0.00	0.00 ± 0.00	0.00 ± 0.00	0.00 ± 0.00	0.00 ± 0.00
Synthesized GLE-ZNO NP	12.62 ± 0.50	19.99 ± 0.20	10.80 ± 0.53	17.72 ± 0.12	35.55 ± 3.85
Untreated RY-86	28.72 ± 0.50	60.45 ± 0.90	25.00 ± 0.93	51.10 ± 0.80	62.22 ± 3.85
Untreated RB-220	22.11 ± 0.50	55.48 ± 0.44	15.12 ± 0.53	45.23 ± 0.26	64.44 ± 3.84
Untreated RB-222	31.30 ± 1.00	65.14 ± 0.46	59.87 ± 2.14	59.55 ± 0.12	57.77 ± 3.85
Untreated R-120	74.70 ± 0.50	71.49 ± 0.26	31.48 ± 0.93	66.58 ± 0.19	51.11 ± 3.85
Treated RY-86	4.29 ± 0.00	14.84 ± 0.00	10.80 ± 0.53	12.81 ± 0.07	28.88 ± 3.85
Treated RB-220	10.61 ± 0.50	9.41 ± 0.50	7.40 ± 0.00	9.36 ± 0.33	4.44 ± 3.85
Treated RB-222	19.81 ± 0.00	18.48 ± 0.35	20.37 ± 0.00	18.97 ± 0.25	4.44 ± 3.85
Treated R-120	14.06 ± 0.50	14.32 ± 0.60	6.48 ± 0.00	13.64 ± 0.19	8.88 ± 3.85

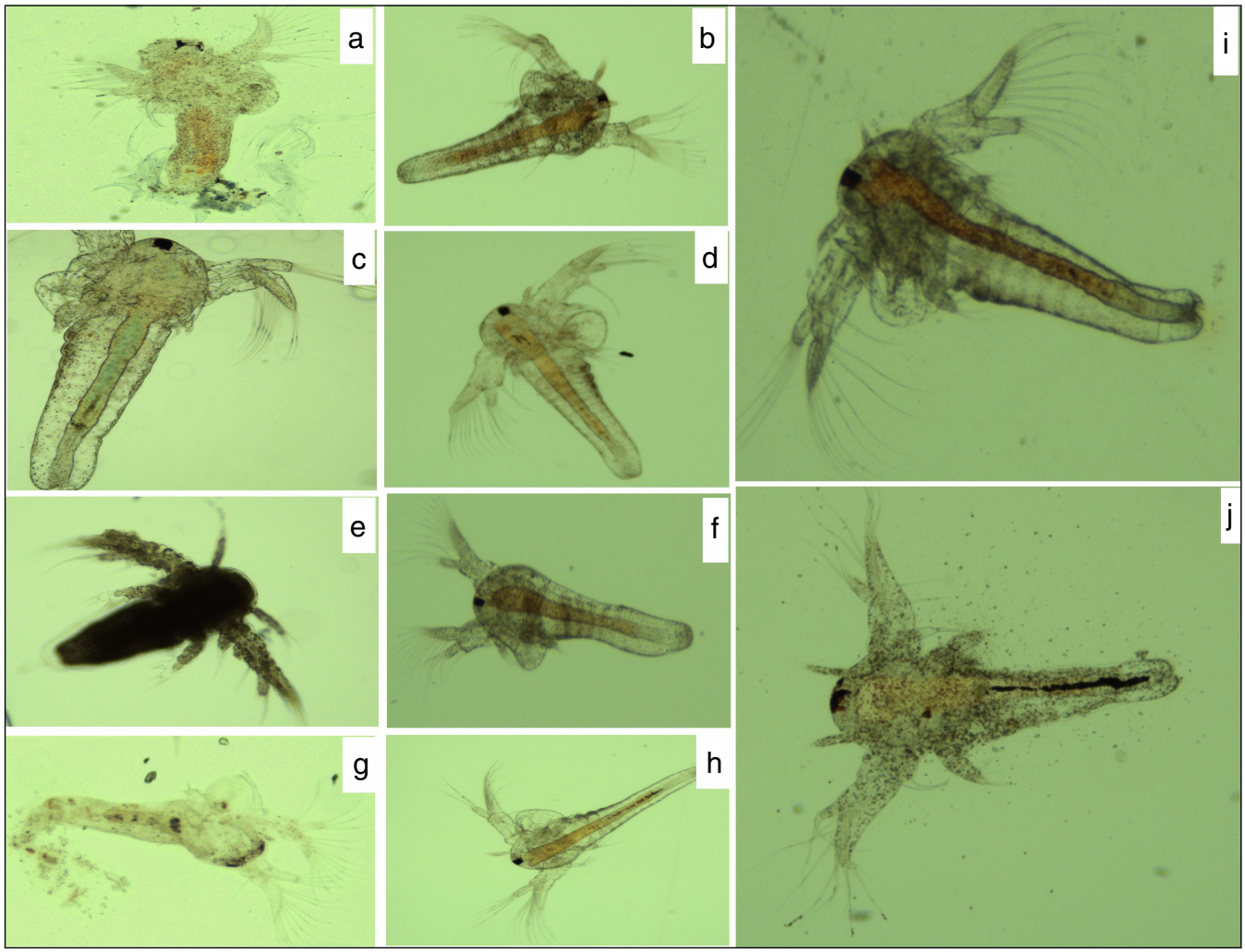

Fig. 11. Microscopic images of brine shrimp nauplii exposed to distilled water, GLE-ZNO NPs, untreated and NP treated dye solutions; (a) untreated RY-86, (b) NP treated RY-86, (c) untreated RB-220, (d) NP treated RB-220, (d) untreated RB-222, (f) NP treated RB-222, (g) untreated R-120, (h) NP treated R-120, (i) distilled water, (j) GLE-ZnO NPs

similar observation as nauplii exposed to distilled water suggesting the efficient degradation of dye molecules by the biosynthesized GLE-ZnO NPs.

Conclusion

The study investigated the potential of *Garcinia gummi-gutta* leaves extract in the bioreduction synthesis of ZnO nanoparticles. The synthesized ZnO nanoparticles were characterized by different spectroscopic and microscopic techniques. The SEM and TEM analysis of the GLE-ZnO NPs revealed the hexagonal shaped nanoparticles of size 72.78 nm and 71.91 nm, respectively. The GLE-ZnO NPs were efficiently used as photocatalysts in the degradation of reactive textile dyes and the photodegradation efficiency was analyzed by investigating the toxicity on *Vigna radiata* sprouts and brine shrimp nauplii. The antimicrobial potential as well as the anticancer potential of GLE-ZnO NPs were also successfully evaluated.

CONFLICT OF INTEREST

The authors declare that there is no conflict of interests regarding the publication of this article.

REFERENCES

1. S. Ahmed, Annu, S.A. Chaudhry and S. Ikram, *J. Photochem. Photobiol. B: Biology*, **166**, 272 (2017); https://doi.org/10.1016/j.jphotobiol.2016.12.011
2. T. Varadavenkatesan, E. Lyubchik, S. Pai, A. Pugazhendhi, R. Vinayagam and R. Selvaraj, *J. Photochem. Photobiol. B*, **199**, 111621 (2019); https://doi.org/10.1016/j.jphotobiol.2019.111621
3. J.T. Kurian, P. Chandran and J.K. Sebastian, *J. Clust. Sci.*, **34**, 2229 (2023); https://doi.org/10.1007/s10876-022-02403-6
4. P.C. Nagajyothi, S.V. Prabhakar Vattikuti, K.C. Devarayapalli, K. Yoo, J. Shim and T.V.M. Sreekanth, *Crit. Rev. Environ. Sci. Technol.*, **50**, 2617 (2020); https://doi.org/10.1080/10643389.2019.1705103
5. A. Khanna and V.K. Shetty, *Sol. Energy*, **99**, 67 (2014); https://doi.org/10.1016/j.solener.2013.10.032
6. Z.H. Mahmoud, M.S. Falih, O.E. Khalaf, M.A. Farhan and F.K. Ali, *J. Adv. Pharm. Educ. Res.*, **8**, 51 (2018).
7. R. Rathnasamy, P. Thangasamy, R. Thangamuthu, S. Sampath and V. Alagan, *J. Mater. Sci. Mater. Electron.*, **28**, 10374 (2017); https://doi.org/10.1007/s10854-017-6807-8
8. J. Gangwar and J.K. Sebastian, *Water Sci. Technol.*, **84**, 3286 (2021); https://doi.org/10.2166/wst.2021.430
9. A. Kumar, S.R. Shah, T.J. Jayeoye, A. Kumar, A. Parihar, B. Prajapati, S. Singh and D.U. Kapoor, *Front. Nanotechnol.*, **5**, 1175149 (2023); https://doi.org/10.3389/fnano.2023.1175149

10. J. Puthukulangara Jaison and J. Kadanthottu Sebastian, *Water Pract. Technol.*, **18**, 911 (2023); https://doi.org/10.2166/wpt.2023.041
11. V. Batra, I. Kaur, D. Pathania, Sonu and V. Chaudhary, *Appl. Surf. Sci. Adv.*, **11**, 100314 (2022); https://doi.org/10.1016/j.apsadv.2022.100314
12. T. Shabatina, O. Vernaya, A. Shumilkin, A. Semenov and M. Melnikov, *Materials*, **15**, 3602 (2022); https://doi.org/10.3390/ma15103602
13. U.L. Ifeanyichukwu, O.E. Fayemi and C.N. Ateba, *Molecules*, **25**, 4521 (2020); https://doi.org/10.3390/molecules25194521
14. K. Elumalai and S. Velmurugan, *Appl. Surf. Sci.*, **345**, 329 (2015); https://doi.org/10.1016/j.apsusc.2015.03.176
15. J.P. Jaison, B. Balasubramanian, J. Gangwar, N. James, M. Pappuswamy, A.V. Anand, N.A. Al-Dhabi, M.V. Arasu, W.-C. Liu and J.K. Sebastian, *Antibiotics*, **12**, 543 (2023); https://doi.org/10.3390/antibiotics12030543
16. N.A. Sarip, N.I. Aminudin and W.H. Danial, *Environ. Chem. Lett.*, **20**, 469 (2022); https://doi.org/10.1007/s10311-021-01319-3
17. M. Mannarmannan and K. Biswas, *ChemistrySelect*, **4**, 12739 (2019); https://doi.org/10.1002/slct.201903159
18. A.R. Pai, A.M. Pillai, A. Jayapraksh and A. John, *Nano Biomed. Eng.*, **8**, 288 (2016); https://doi.org/10.5101/nbe.v8i4.p288-296
19. S.M. George and T. Senthilnathan, *Sens. Lett.*, **15**, 156 (2017); https://doi.org/10.1166/sl.2017.3783
20. M. Raghavendra, K.V. Yatish and H.S. Lalithamba, *Eur. Phys. J. Plus*, **132**, 358 (2017); https://doi.org/10.1140/epjp/i2017-11627-1
21. E. Gurgur, S.S. Oluyamo, A.O. Adetuyi, O.I. Omotunde and A.E. Okoronkwo, *SN Appl. Sci.*, **2**, 911 (2020); https://doi.org/10.1007/s42452-020-2269-3
22. M. Balouiri, M. Sadiki and S.K. Ibnsouda, *J. Pharm. Anal.*, **6**, 71 (2016); https://doi.org/10.1016/j.jpha.2015.11.005
23. F.D. Gonelimali, J. Lin, W. Miao, J. Xuan, F. Charles, M. Chen and S.R. Hatab, *Front. Microbiol.*, **9**, 1639 (2018); https://doi.org/10.3389/fmicb.2018.01639
24. F. Denizot and R. Lang, *J. Immunol. Methods*, **89**, 271 (1986); https://doi.org/10.1016/0022-1759(86)90368-6
25. M. Frei, *BioFiles Online*, **6**, 17 (2011).
26. P. Jishma, T. Roshmi, S. Snigdha, and E. K. Radhakrishnan, *3 Biotech*, **8**, 97 (2018); https://doi.org/10.1007/s13205-018-1116-3
27. M. Bilal, M. Iqbal, H. Hu and X. Zhang, *Water Sci. Technol.*, **73**, 2332 (2016); https://doi.org/10.2166/wst.2016.082
28. N. Supraja, T. Prasad, A.D. Gandhi, D. Anbumani, P. Kavitha and R. Babujanarthanam, *Biochem. Biophys. Rep.*, **14**, 69 (2018); https://doi.org/10.1016/j.bbrep.2018.04.004
29. D. Jain, A.A. Shivani, A.A. Bhojiya, H. Singh, H.K. Daima, M. Singh, S.R. Mohanty, B.J. Stephen and A. Singh, *Front Chem.*, **8**, 778 (2020); https://doi.org/10.3389/fchem.2020.00778
30. A.M. Abdo, A. Fouda, A.M. Eid, N.M. Fahmy, A.M. Elsayed, A.M.A. Khalil, O.M. Alzahrani, A.F. Ahmed and A.M. Soliman, *Materials*, **14**, 6983 (2021); https://doi.org/10.3390/ma14226983
31. M. Rafique, R. Tahir, S.S.A. Gillani, M.B. Tahir, M. Shakil, T. Iqbal and M.O. Abdellahi, *Int. J. Environ. Anal. Chem.*, **102**, 23 (2022); https://doi.org/10.1080/03067319.2020.1715379
32. M. Aminuzzaman, L.P. Ying, W.-S. Goh and A. Watanabe, *Bull. Mater. Sci.*, **41**, 50 (2018); https://doi.org/10.1007/s12034-018-1568-4
33. B.S. Jena, G.K. Jayaprakasha, R.P. Singh and K.K. Sakariah, *J. Agric. Food Chem.*, **50**, 10 (2002); https://doi.org/10.1021/jf010753k
34. A. Rajan, M. MeenaKumari and D. Philip, *Spectrochim. Acta A Mol. Biomol. Spectrosc.*, **118**, 793 (2014); https://doi.org/10.1016/j.saa.2013.09.086
35. J. Jiang, G. Oberdörster and P. Biswas, *J. Nanopart. Res.*, **11**, 77 (2009); https://doi.org/10.1007/s11051-008-9446-4
36. S. Yedurkar, C. Maurya and P. Mahanwar, *J. Open Synth. Theory Appl.*, **5**, 1 (2016); https://doi.org/10.4236/ojsta.2016.51001
37. L. Wang, Y. Wu, J. Xie, S. Wu and Z. Wu, *Mater. Sci. Eng. C*, **86**, 1 (2018); https://doi.org/10.1016/j.msec.2018.01.003
38. N. Saadat and S.V. Gupta, *J. Oncol.*, **2012**, 647206 (2012); https://doi.org/10.1155/2012/647206
39. A. Umamaheswari, S.L. Prabu, S.A. John and A. Puratchikody, *Biotechnol. Rep.*, **29**, e00595 (2021); https://doi.org/10.1016/j.btre.2021.e00595